



## The effect of Cr concentration on radiation damage in Fe–Cr alloys

K. Vörtler<sup>a,\*</sup>, C. Björkas<sup>a</sup>, D. Terentyev<sup>b</sup>, L. Malerba<sup>b</sup>, K. Nordlund<sup>a</sup>

<sup>a</sup> Association Euratom-TEKES, Department of Physics, University of Helsinki, P.O. Box 43, FI-00014, Finland

<sup>b</sup> SCK-CEN, the Belgian Nuclear Research Centre, Boeretang 200, B-2400 Mol, Belgium

### ARTICLE INFO

#### Article history:

Received 13 February 2008

Accepted 2 September 2008

#### PACS:

61.72.Ji

61.80.Hg

28.52.Fa

34.20.Cf

### ABSTRACT

Displacement cascades in Fe–Cr alloys were studied using molecular dynamics computer simulations. We considered random Fe–5Cr and Fe–15Cr alloys, as well as Fe–10Cr alloys with and without Cr-rich precipitates. In the simulations two versions of a two-band embedded atom method potential were used, and the cascades were induced by recoils with energies up to 20 keV. We found that the average number of surviving Frenkel pairs and the fraction of vacancies and self-interstitials in clusters was approximately the same in pure Fe and random Fe–Cr alloys (regardless of Cr concentration). A noticeable effect of the presence of Cr in the Fe matrix was only observed in the enrichment of self-interstitials by Cr in Fe–5Cr. The calculated change in the short range order parameter showed that Fe–5Cr tends towards ordering (negative short range order parameter) and Fe–15Cr towards segregation (positive short range order parameter) of Cr atoms. In simulations with the Cr-rich precipitate, enhanced cascade splitting and segregation of self-interstitial defects created inside the precipitates towards the precipitate–matrix interface region was observed. The number of Frenkel pairs and their clustered fraction was not affected by the presence of the precipitate.

© 2008 Elsevier B.V. All rights reserved.

### 1. Introduction

Ferritic/martensitic (FM) steels are candidate structural materials for advanced near-future fission and future fusion reactors [1]. High-Cr FM steels for nuclear applications (including reduced activation and oxide-dispersed strengthened) typically contain from 7 to 14 at.% Cr, while the content of the other alloying elements generally does not exceed 1–2%. The choice of these steels is governed by their superior resistance to neutron irradiation, in terms of low damage accumulation and swelling, compared to e.g. austenitic steels [2–5]. Nonetheless, in future nuclear systems it is expected that core structural materials will be subjected to severe irradiation and environmental conditions during the reactor life-time [1]. A quantitative understanding of the mechanisms leading to the change of properties of these steels after long-term exposure to irradiation is therefore recognized to be of high importance for a safe design and operation of innovative nuclear systems [6]. A great deal of understanding can be achieved by studying simpler model systems such as, in the case of high-Cr steels, Fe–Cr alloys.

The degradation of material properties under irradiation is a multi-scale phenomenon, meaning that different physical processes take place on different time and space levels. Nowadays, it is widely accepted that a multi-scale modelling approach provides a practical framework to tackle this problem. This approach begins with the production of atomic-scale defects by individual displacement

cascades and ends with plasticity and fracture mechanics treatment of whole components, wherein the response of the material to changes in temperature and/or applied stress is of concern [7]. In this framework, molecular dynamics (MD) techniques are a unique tool for studying the primary damage state due to displacement cascades induced by high energy particles (such as neutrons, ions, electrons, etc.). Over the last decade MD simulations have been widely used to assess the primary damage state in pure bcc Fe [8], some Fe-based systems [9–11], and also Fe–Cr alloys [12–16]. Simulations of displacement cascades in Fe–Cr random alloys have been carried out mostly in Fe–10Cr alloys [12–15], with the exception of the work by Wallenius et al. [16], where Fe–5Cr and Fe–20Cr were studied as well. Although different interatomic potentials were used in the above-cited works, the following common conclusions were drawn about the effect of Cr on the primary damage state in Fe–Cr alloys:

- (i) The presence of Cr hardly affects the number of formed Frenkel pairs and their distribution in clusters as compared to pure Fe.
- (ii) Self-interstitial atoms (SIAs) and their clusters were observed to be enriched by Cr atoms, due to the presence of sufficiently high binding energy between a Cr atom and a SIA (in both  $\langle 110 \rangle$  and  $\langle 111 \rangle$  configurations).

It should be mentioned, however, that most of the previously used potentials suffered from an incorrect description of SIA properties in Fe [17] and the mixing enthalpy of the Fe–Cr system

\* Corresponding author. Tel.: +358 9 19150088; fax: +358 9 19150042.  
E-mail address: [katharina.vortler@helsinki.fi](mailto:katharina.vortler@helsinki.fi) (K. Vörtler).

[18,19], when compared with available data obtained from first principle calculations. Since the latter was not reproduced, earlier simulations could only be reliably performed for a Cr concentration ( $C_{Cr}$ ) of 10%, since this was the only concentration that was acceptably described. The work by Björkas et al. [13] is the only exception; there, recent two-band model Fe–Cr potentials [20] were used. These potentials were especially fitted to reproduce the heat of mixing of Fe–Cr alloys in the whole range of Cr concentrations according to density functional theory (DFT) data. They also reproduce reliably SIA properties in Fe [17] and Fe–Cr [20,21]. The study of alloys with other  $C_{Cr}$  (both less and more than 10%) is of importance since there exists a change in the short range-order (SRO) parameter from negative to positive at about 10%, at 700 K [22]. Consequently, if  $C_{Cr}$  exceeds a critical concentration ( $\sim 10\%$  at 700 K) in binary Fe–Cr alloys, as well as in FM steels, the  $\alpha$ - $\alpha'$  phase separation occurs after thermal ageing or under irradiation, resulting in the formation of finely dispersed, nanometer size, matrix-coherent Cr-rich precipitates [23,24]. On the other hand, in alloys with  $C_{Cr} < 10\%$  a tendency towards ordering of Cr atoms is experimentally detected [22,25]. Note that both of these processes take place in the region of temperatures potentially important for technological applications (above 600 K). Moreover, phase transformation can be accelerated under irradiation [23,24] due to self diffusion via radiation-induced defects and, possibly, also to direct in-cascade atomic redistribution.

In this work, we study the primary damage state in Fe–Cr binary alloys with different Cr content, addressing the following issues:

- (i) Is it still true, that the presence of Cr does not affect the number of formed Frenkel pairs and their clustering in alloys different from Fe–10Cr, characterized by different thermodynamic properties?
- (ii) Is the in-cascade ballistic mixing sufficient to induce, within the short time frame of the cascade, Cr atom redistribution as dictated by the acting thermodynamic forces (i.e. the heat of mixing of the corresponding alloy)?
- (iii) Do cascades dissolve pre-existing Cr precipitates, contribute to their growth, or in any way modify them? Do precipitates affect the primary damage state due to the cascades initiated near them?

To address issues (i) and (ii), displacement cascades were simulated in Fe–5Cr and Fe–15Cr alloys, where Cr atoms were distributed randomly. The evolution of cascades in Fe–12Cr alloys containing Cr-rich precipitates was studied as well, to address issue (iii). The simulations were carried out using two versions of the two-band potential from Ref. [20], fitted to different sets of the heat of mixing obtained from DFT. Thus, we also examine the effect of the mixing enthalpy, to which the potentials were fitted, on the primary damage state in Fe–5Cr and Fe–15Cr alloys.

## 2. Method

### 2.1. Displacement cascades in Fe–5Cr and Fe–15Cr

As mentioned above, for the MD simulations of displacement cascades in Fe–Cr alloys we used two two-band (2B) EAM (embedded atom model) potentials [20], that were fitted to two different mixing enthalpy data sets, obtained from different *ab initio* methods. These two classical potentials are here referred to with the abbreviations of the corresponding *ab initio* methods used for the mixing enthalpy calculation [18,19]. These are ‘EMTO’ and ‘PAW’, that stand for the Exact Muffin–Tin Orbital [26] and Projector Augmented Wave [27,28] methods, respectively. A more detailed description of the development of these potentials can be found in Ref. [20].

The cascade simulations were performed using the PARCAS code [29]. The simulation cell size, number of events, simulation time, and recoil energy can be found in Table 1. The initial simulation box consisted of randomly distributed Fe–5Cr and Fe–15Cr, respectively. Periodic boundary conditions [30] in all three dimensions were used. No electronic stopping was applied [31], to be consistent with most previous works for Fe–Cr [12,13]. Initially the simulation cells were equilibrated at zero pressure for 10 ps at 300 K using Berendsen pressure and temperature control [32]. The primary knock-on atom (PKA) was an Fe atom near the center of the cell. The direction of the recoil was random. Temperature scaling (with a constant of 100 fs) was applied in the cell’s border regions (with a thickness of one lattice parameter). The simulation was stopped if the kinetic energy of a border atom was larger than 10 eV and restarted with the recoil atom placed farther away from the border. To fulfil this criterion at  $E_{PKA} = 20$  keV, approximately five runs out of 15 were repeated in a larger simulation cell containing 1,458,000 atoms.

To analyze the defects a Wigner-Seitz cell, centered at each lattice site, was used: an empty cell corresponded to a vacancy, while two atoms in the same cell were a self-interstitial configuration. We performed a cluster connectivity analysis, which means that a group of defects are interpreted to belong to the same cluster if they are within a given distance from at least one other defect of the same type. This distance is called a (clustering) cut-off radius. The choice of the cut-off radius is governed by the presence of some significant binding energy between alike defects, which is the 2nd nearest neighbor (nn) for vacancy defects, and the 3rd nn for SIA defects. Special attention was paid to the fraction of clustered SIAs and vacancies, as well as to the Cr content among SIAs and clustered SIAs.

The ordering of the alloy was analyzed. We used the SRO parameter definition by Cowley [33]. The average SRO parameter within the 2nd nn shell was calculated for the number of atoms  $N_h$ , that belong to the cascade during the heat spike phase; the average SRO is therefore independent of the simulation cell size.

**Table 1**

The recoil energy, time of simulation, number of events, box size, and number of atoms used in randomly distributed Fe–5Cr and Fe–15Cr

Energy (keV)	Simulation time (ps)	Number of events				Box size ( $a_0$ )	Number of atoms
		Fe–5Cr		Fe–15Cr			
		EMTO	PAW	EMTO	PAW		
0.5	20	20	20	20	20	20	16000
1	20	20	20	20	20	25	31250
2	20	20	20	20	20	31	59582
5	20	20	100	20	100	42	148176
10	25	15	15	15	15	54	314928
20	25	15	15	15	15	67	601526

The EMTO and the PAW potentials are versions of the potential by Olsson et al. [20].

An atom was labeled to belong to the heat spike if the average energy of it and its nearest neighbors was higher than 0.234 eV (the melting point of the material in units of eV). The change in SRO was calculated for the simulation cell before and after the cascade.

## 2.2. Cascades with and without Cr precipitates

The simulation of displacement cascades in Fe–10Cr matrices with and without Cr-rich precipitates was performed using the MD code DYMOKA [34], wherein the PAW potential is implemented and used for this purpose. We have earlier cross-checked that the PARCAS and DYMOKA codes give fully consistent results [13]. The simulation cells were prepared as follows. A Cr-rich precipitate with a diameter of 5 nm and containing 95% Cr was placed at the center of a simulation box. The size of this box was  $50 \times 50 \times 50 \times a_0^3$  ( $a_0$  is the equilibrium lattice parameter for Fe–10Cr at 300 K), and it initially contained 10% of randomly distributed Cr atoms. In this cell the precipitate was created by changing randomly with a probability of 95% the atoms in a spherical volume to Cr. The total concentration of Cr in the matrix, including Cr atoms in the precipitate, was  $\sim 12\%$  Cr. Prior to initiating the cascade, the cell was equilibrated for 10 ps at 300 K. It was then used as starting point for the cascade simulation and as reference for defect detection. The cascade was initiated by imparting a kinetic energy,  $E_{PKA}$ , to a certain PKA along a high-index direction, such as  $\langle 135 \rangle$ . The recoil was also directed towards the center of the precipitate. We used a variable MD time step, that can change in the range from 0.001 to 5 fs. We simulated 20 keV cascades in the matrix with and without the precipitate using different initial positions of the PKA for every cascade. After equilibrium to the desired temperature, all simulations were performed in the NVE microcanonical ensemble, applying periodic boundary conditions. We simulated a total number of 10 cascades both with and without precipitate.

The evolution of the cascade was followed by studying selected representative snapshots. Intermediate and final atomic configurations were analyzed to detect and count defects, using the Wigner-Seitz cell method (see Section 2.1). Such analysis allowed the self-interstitial orientation (i.e.  $\langle 110 \rangle$  or  $\langle 111 \rangle$ ) and its chemical composition to be identified. The defect distribution and evolution were monitored using appropriate visualization tools, and defect clusters were detected using an automated procedure.

## 3. Results

### 3.1. Displacement cascades in Fe–5Cr and Fe–15Cr

#### 3.1.1. Survived defects

The average number of surviving Frenkel pairs in cascades simulated in Fe–5Cr and Fe–15Cr alloys is shown in Fig. 1. It can be seen, that the number of survived defects increases with PKA energy and, at the same time, the slope of the curve is essentially the same as for the data obtained for pure Fe, using the Ackland–Mendelev–Srolovitz (AMS) potential [35] denoted as AMS Fe in Fig. 1. Thus, the presence of 5 and 15% of randomly distributed Cr atoms does not affect the total number of survived Frenkel pairs, that is found to be the same as in pure Fe and in Fe–10Cr [12,13]. The fraction of vacancies and self-interstitials in clusters is presented in Figs. 2 and 3. The fraction of clustered vacancies is approximately constant, within scatter, over the whole range of PKA energy, independently of the Cr content in the alloy. The values of vacancy clustered fraction in the alloys and in pure Fe (added for comparison) lay between 0.3 and 0.5. The fraction of SIAs in clusters is lower than that of vacancies for PKA energies smaller than 20 keV. It grows with PKA energy, reaching 0.5 for  $E_{PKA} = 20$  keV, where it is equal to the clustered fraction of vacan-

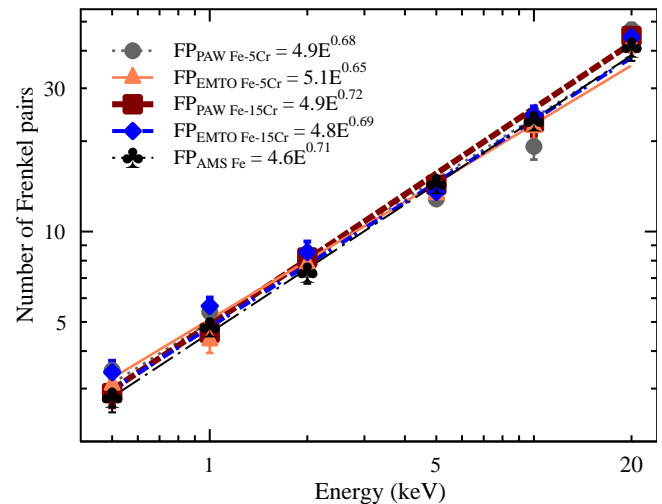


Fig. 1. The average number of surviving Frenkel pairs as a function of recoil damage energy obtained by cascade simulations in Fe–Cr, and in pure Fe using the AMS potential [13,35]. The relationship for Frenkel pairs  $FP = A(E_{PKA})^m$  by Bacon et al. [40] is included. The error bars give the  $1\sigma$  standard error of the average.

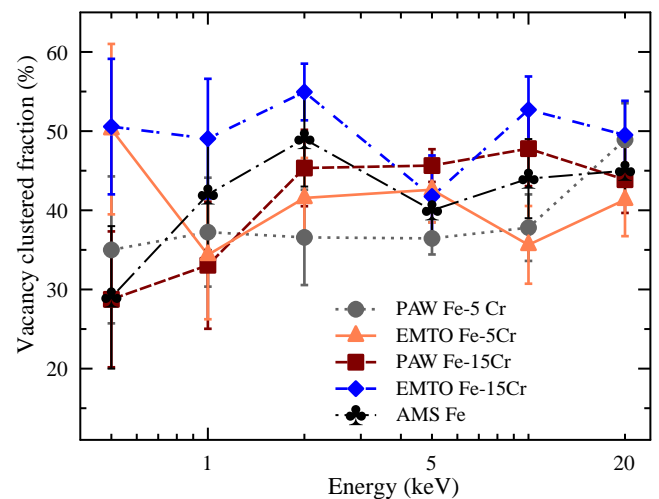
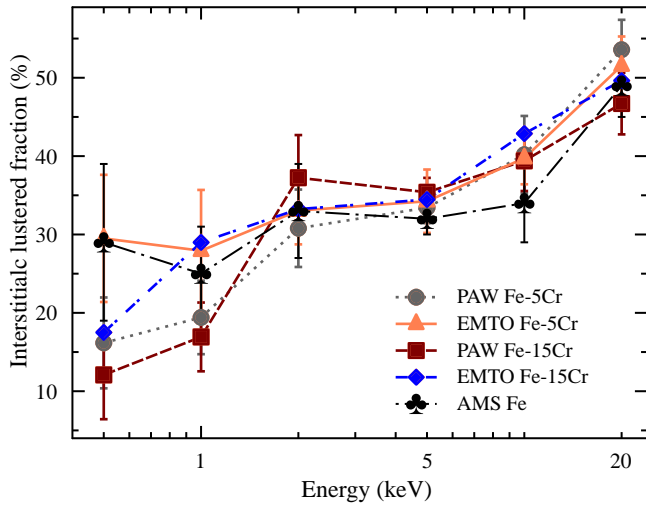


Fig. 2. The fraction of vacancies in clusters obtained by cascade simulations in Fe–Cr, and in pure Fe using the AMS potential [13,35]. The error bars give the  $1\sigma$  standard error of the average.

cies (see Fig. 3). Again, one can see that the effect of Cr is insignificant. The variations between the different potentials are also small.

The number of Cr atoms associated with survived self-interstitial defects was analyzed together with the previously published data for Fe–10Cr alloys [13]. The ratio between the Cr content in SIA defects and the average Cr concentration in the matrix is presented in Fig. 4. The data set obtained with the PAW potential shows that there is a significant enrichment of SIA defects by Cr: the Cr content in SIAs exceeds 2.5 times the matrix composition in Fe–5Cr and 1.5 times in Fe–10Cr alloys. The enrichment of SIAs by Cr is especially pronounced in cascades of low PKA energy. The results obtained with the EMTO potential show that SIAs are enriched by Cr only in the Fe–5Cr alloy, where the Cr content associated to the SIA defects approximately exceeds two times the matrix content in the whole range of PKA energy. Small enrichment was also observed in the Fe–10Cr alloy in cascades with  $E_{PKA}$  above 5 keV. In the Fe–15Cr alloy, the formed SIA defects were found to be depleted by Cr atoms, although only slightly. In addi-



**Fig. 3.** The fraction of SIAs in clusters obtained by cascade simulations in Fe–Cr, and in pure Fe using the AMS potential [13,35]. The error bars give the  $1\sigma$  standard error of the average.

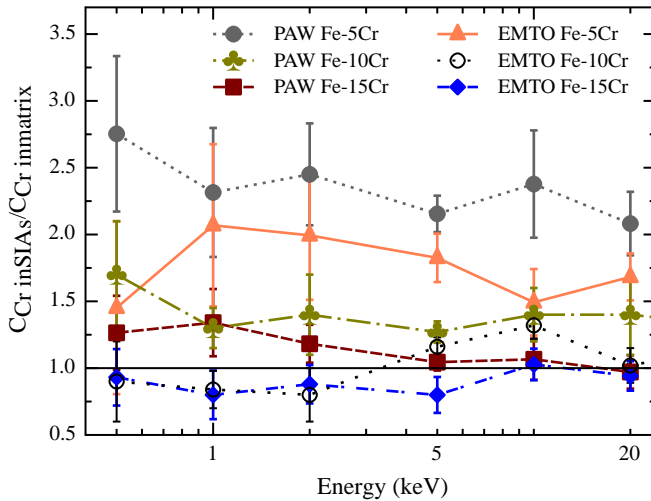


**Fig. 4.** Ratio of the Cr content in SIAs over the Cr content in the Fe–Cr matrix obtained by cascade simulations. The corresponding values for Fe–10Cr [13] have been added. The error bars give the  $1\sigma$  standard error of the average.

tion, the Cr content in one-dimensionally mobile SIA clusters (i.e. containing more than 5 SIAs [36]) was analyzed separately and the results are presented in Fig. 5. Due to the high affinity of Cr to the  $\langle 111 \rangle$  SIAs (which form the 1D-migrating clusters [37,38]) these clusters may be expected to be enriched by Cr in Fe–5Cr alloys. This, however, cannot be stated from the results presented in Fig. 5, especially taking into account the large statistical errors (due to the limited number of clusters formed in cascades). Thus, the main contribution to the enrichment of SIAs by Cr in Fe–Cr alloys is to be attributed to the single SIAs and small 3D-migrating SIA clusters. Possible reasons for this are discussed in Section 4.

### 3.1.2. Short range ordering

The change of the SRO parameter was calculated in matrices subjected to cascades initiated by a PKA with an energy of 5 keV and simulated using the PAW potential. For the sake of statistical accuracy of the results, 100 cascades were simulated in Fe–5Cr and Fe–15Cr alloys. The change of the SRO parameter for the atoms in the cascade is shown in Table 2 for Fe–5Cr and Fe–15Cr alloys together with the value for Fe–10Cr, obtained using the PAW po-

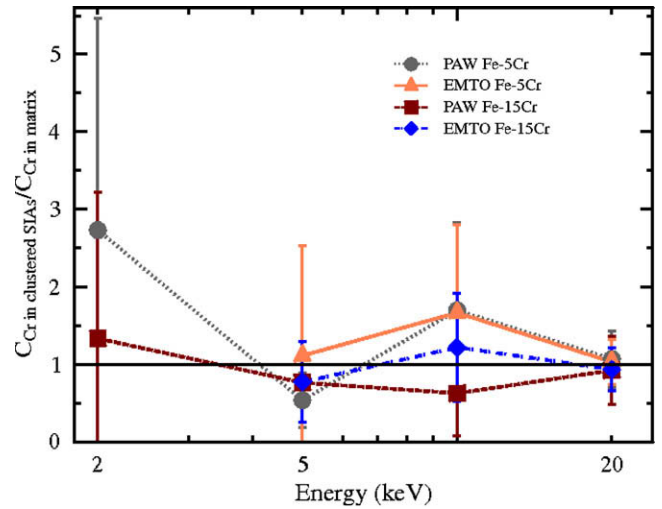


**Fig. 5.** Ratio of the Cr content in clustered SIAs over the Cr content in the Fe–Cr matrix. Only clusters containing at least 5 defects were considered. The error bars give the  $1\sigma$  standard error of the average. For 2 keV they are large, since very few large clusters were formed at this energy.

**Table 2**

Change in SRO parameter in 5 keV cascades using the PAW potential

	Fe–5Cr	Fe–10Cr	Fe–15Cr
$\Delta$ SRO	$-0.0023 \pm 0.0006$	$-0.0006 \pm 0.0013$	$0.0041 \pm 0.0007$
1st shell $\Delta$ SRO	$-0.0027 \pm 0.0008$	$0.0013 \pm 0.0009$	$0.0053 \pm 0.0009$
$N_{hs}$	$4630 \pm 20$	$4650 \pm 30$	$4680 \pm 20$

The average of  $\Delta$ SRO was only calculated for the number of atoms belonging to the cascade's heat spike  $N_{hs}$ . The  $1\sigma$  standard error of the average is given.

tential in Ref. [13]. Although the total change of the SRO parameter is fairly small, its absolute value is larger than the estimated standard errors, except in Fe–10Cr, thereby revealing that no net SRO change is induced by a cascade in this alloy. The initially random Fe–5Cr alloy tends towards ordering (negative SRO parameter), while segregation of Cr atoms occurs in the initially random Fe–15Cr (positive SRO parameter). Note that the contribution to the SRO parameter change in the Fe–5Cr alloy is mainly due to the redistribution of 1st nn pairs (see data in Table 2). In this alloy 1st nn Cr–Cr pairs break up to form additional 1st nn Fe–Cr pairs. In the Fe–15Cr alloy Cr clusters (consisting of both 1st and 2nd nn atoms) tend to form and/or grow. Thus, a redistribution of atoms leading to a change of the value of the SRO parameter is proven to occur even within the very short time frame (a few ps) of the ballistic and relaxation phases of the cascade, without contribution from thermally activated diffusion of cascade-induced defects. From the current simulations it is, however, not possible to determine the total extent of ordering and clustering during prolonged irradiation. This is because diffusive processes may on long time-scales counteract or enhance the change in short-range order produced in individual collision cascades.

### 3.2. Effect of Cr-rich precipitates on the primary damage state in Fe–10Cr

#### 3.2.1. Effect on the cascade morphology

A typical cascade consists of at least two main phases: the ballistic phase (when atoms collide and the number of defects grows in time) and the relaxation phase (when recombination of opposite types of defects and the formation of clusters made by alike defects occurs, in dense materials also known as the heat spike phase) [39].

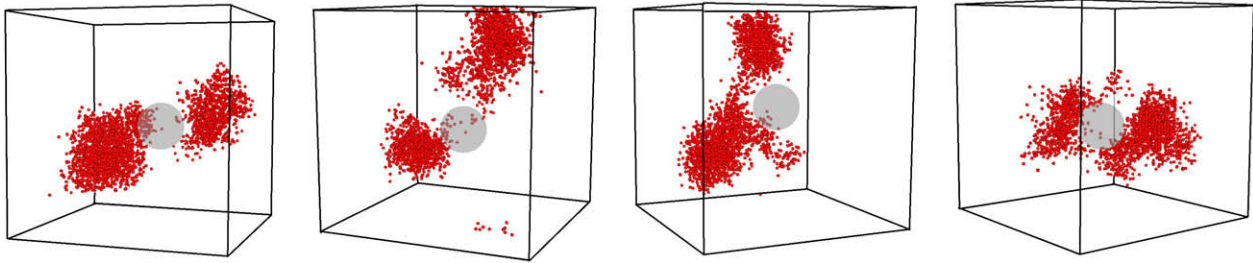


**Fig. 6.** The appearance at peak time of four typical 20 keV cascades in a Fe–10Cr alloy with a Cr-rich precipitate. Small red balls indicate positions of self-interstitials, while the grey sphere in the center of the box shows the position (and size) of the precipitate.

Fig. 6 shows four snapshots of four 20 keV cascades in an Fe–10Cr matrix, containing a 5 nm Cr-rich precipitate (shown as a grey sphere) placed in the center of the box, and self-interstitial defects (shown as small red balls). The snapshots were extracted from simulations at the moment when the largest number of Frenkel pairs is produced, i.e. at the moment when the ballistic phase is finished and the recombination phase starts (peak time). It can be seen from the figure, that each cascade is split into two or more sub-cascades and only few self-interstitials are present in the precipitate region. Similar visual inspection of other simulated cascades has revealed that almost every cascade was split near the precipitate, while only 50% of the cascades initiated in the Fe–10Cr matrix (without the precipitate) formed sub-cascades, suggesting that the presence of the Cr-rich precipitate provokes cascade splitting. At the end of the relaxation stage (i.e. after more than 20 ps), when the amount of survived defects becomes constant, the pre-existing precipitates were not dissolved and the size and shape of the precipitates remained unchanged, as it was also revealed by atomic visualization tools.

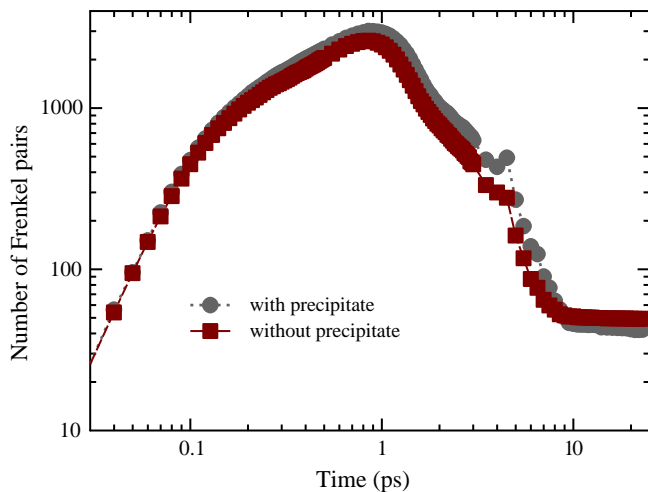


**Fig. 7.** The average number of Frenkel defects versus simulation time of two individual cascades initiated by 20 keV PKAs in Fe–10Cr without (squares) and with (circles) the precipitate.

By monitoring the spatial distribution of the defects in matrices containing precipitates versus elapsed time, we observed that most of the self-interstitial defects initially formed in the precipitates escaped to the precipitate–matrix interface during the relaxation phase. This SIA segregation to the interface is related to the substantial difference in the formation energy of SIAs in the precipitate and in the matrix. Indeed, the average formation energy of a  $\langle 110 \rangle$  dumbbell in Fe–10Cr matrix was calculated to be 3.3 eV, whereas in the Cr-rich precipitate (95% Cr) it is 5.5 eV, using the PAW potential (see Ref. [21]). Accordingly, almost no isolated SIAs or SIA clusters were observed in the precipitates at the end of the cascades.

The time–evolution of the average number of Frenkel pairs (averaging was performed over the number of simulated cascades) initiated by 20 keV cascades in Fe–10Cr with and without the precipitate is presented in Fig. 7. A slightly higher number of defects at the end of ballistic stage lingered in the crystal containing the precipitate, which is most likely a result of cascade splitting. Besides this tiny difference, the evolutions of the number of defects are almost identical.

### 3.2.2. Survived defects

After the end of the relaxation stage, the survived defects were characterized in terms of their number, clustered fractions, and chemical nature of self-interstitials. The comparative summary presented in Table 3 shows that the total number of survived Frenkel pairs is slightly higher in the matrix containing the precipitate. The difference, however, is statistically insignificant taking into account the associated standard errors (see Table 3). The identification of the atom species of the SIAs showed that the amount of Fe–Fe self-interstitials is the same and that no formation of Cr–Cr self-interstitials occurred in either case. This is due to the strongly repulsive binding energy (–0.3 eV [21]) between SIA in  $\langle 110 \rangle$  dumbbell configurations and a pair of Cr atoms (positioned at 1st nn positions), as shown in Table 4.

The number of Fe–Cr SIAs was found to be almost twice as high as in the matrix, when the precipitate is present. The reason for this is certainly the segregation of SIAs formed inside the precipitate region, which migrated towards the precipitate–matrix interface and remained there. The fraction of survived vacancies and SIAs in clusters is practically the same in both cases (see Table 3).

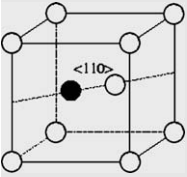
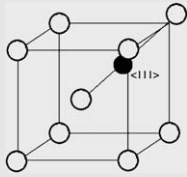
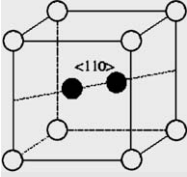
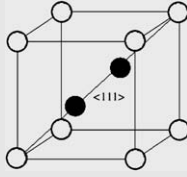
To summarize, the obtained results show that the presence of Cr-rich precipitates does not affect the evolution of the cascade

**Table 3**  
Characterization of defects formed in 20 keV cascades initiated in Fe–10Cr with and without the 5 nm Cr-rich precipitates

	Number of Frenkel pairs	Number of Fe–Fe SIAs	Number of Cr–Cr SIAs	Number of Fe–Cr SIAs	Fraction of Cr in all SIAs	Clustered fraction of SIAs	Clustered fraction of vacancies
With precipitate	49 ± 3	32 ± 2	0 ± 0	17 ± 3	0.17 ± 0.01	0.52 ± 0.03	0.48 ± 0.03
Without	44 ± 3	33 ± 3	0 ± 0	11 ± 1	0.11 ± 0.01	0.50 ± 0.03	0.50 ± 0.03

All values are averaged over the number of simulated cascades and the  $1\sigma$  standard errors are given next to the mean values. SIA stands for self interstitial atom.

**Table 4**  
Binding energy of SIAs with single and Cr–Cr pairs estimated using PAW and EMTO potentials obtained by static atomistic simulations

Configuration	PAW	EMTO	Configuration	PAW	EMTO
	0.14	0.15		0.40	0.37
	−0.29	−0.43		−0.04	−0.21

The energies are given in eV (a positive value means attractive interaction). The methodology used to estimate the binding energy can be found in Ref. [20].

on the ballistic and relaxation stages when it comes to the number of Frenkel defects and their clustered fractions. In turn, the cascade neither dissolved, nor modified in any substantial way the pre-existing precipitate. The main effect of Cr precipitates appears to be the enhancement of the subcascade formation and the segregation of self-interstitial defects initially created inside the precipitates towards the precipitate–matrix interface region.

#### 4. Discussion

The results presented in Section 3.1 show that the chromium content hardly affects the primary damage state in Fe–5Cr, Fe–10Cr, and Fe–15Cr alloys in terms of the number of survived defects and their distribution in clusters, as compared to the previously obtained results in pure Fe [5,12,13]. The results obtained with the two potentials, fitted to a different heat of mixing, are found to be essentially the same with respect to the above mentioned parameters. The number of Frenkel pairs produced per cascade in Fe and the studied Fe–Cr alloys follows the power law dependence for metals proposed by Bacon et al. [40], as illustrated in Fig. 1. The fraction of vacancies in clusters is higher than that of SIAs at low energy and becomes approximately the same at 20 keV (see Figs. 2 and 3), while the SIA clustered fraction grows with PKA energy. Both of these observations are in line with the published data for cascade simulated in pure Fe [12,13] using the same Fe–Fe potential [35].

The enrichment of survived SIA defects by Cr is the main effect detected, but its extent was found to vary depending on the applied Fe–Cr potential (i.e. employing different mixing enthalpies) and PKA energy. Both potentials show significant enrichment of SIAs by Cr formed in cascades simulated in an Fe–5Cr alloy. Furthermore, the enrichment is found to occur in other Fe–Cr alloys as well, when using the PAW potential, whereas the results of cascades simulated with the EMTO potential show very little enrichment in Fe–10Cr (only in high energy cascades with  $E_{PKA} > 5$  keV) and even depletion in the Fe–15Cr alloy. As in Section 3.1.1, no significant enrichment of 1D-migrating SIA clusters was observed in Fe–5Cr and Fe–15Cr with either potential (see Fig. 5). Thus, we conclude that mainly single SIAs and small SIA clusters are enriched by Cr. Previous studies suggest that the origin of the enrichment is the significant binding energy between single SIAs, or small SIA clusters, and Cr atoms [21]. The binding energies of  $\langle 110 \rangle$  and  $\langle 111 \rangle$  self-interstitials with a single Cr atom and Cr–Cr pairs calculated in pure Fe with both applied potentials are given in Table 4. The data presented in the table suggests that the formation of mixed Fe–Cr self-interstitials is energetically favourable, but not

that of Cr–Cr self-interstitials. The binding energies given in Table 4 are, strictly speaking, only relevant in pure Fe or in dilute alloys, where the interference of other Cr atoms can be excluded. In concentrated Fe–Cr alloys, the actual Cr–SIA binding energy depends a lot on the local distribution of the Cr atoms near an SIA and can be both negative or positive [21]. From this point of view, an Fe–5Cr alloy still could be taken as a dilute alloy, since the mean distance between Cr atoms exceeds  $2a_0$ , so the effect of surrounding Cr atoms on the Fe–Cr mixed dumbbell binding energy remains small. In a study of the properties of self-interstitials in Fe–Cr alloys (applying the PAW potential) it was shown that the most frequent self-interstitial configuration in an Fe–5Cr random alloy remains the mixed  $\langle 110 \rangle$  dumbbell [21]. In an Fe–15Cr (random) alloy, on the other hand, the formation of Fe–Cr and Cr–Cr interstitials is less favourable and in general the Fe–Fe  $\langle 110 \rangle$  dumbbell surrounded by Cr atoms has the lowest energy [21]. Thus, with increasing Cr content a kind of saturation of SIA–Cr interaction occurs, so that above a certain concentration the formation of the  $\langle 110 \rangle$  Fe–Fe dumbbells becomes again more favourable than the formation of Fe–Cr dumbbells, which may explain why the enrichment level decreases with increasing Cr content in the studied alloys. Another feature of the enrichment of SIAs by Cr is the dependence on the PKA energy. As seen from Fig. 4, the higher the PKA energy, the lower the enrichment. This may be related to the increase of the fraction of the SIA clusters, which grows with PKA energy. The Cr content in large SIA clusters is the same as in the matrix (Fig. 5). With increasing PKA energy, the fraction of single SIAs becomes smaller, leading to a decrease in the enrichment level.

The change in the SRO parameter, that was found to be statistically meaningful (see Section 3.1.2), is another effect of Cr composition. We showed that the ballistic mixing leads to a redistribution of atoms inducing the change of the SRO parameter, becoming negative in Fe–5Cr and positive in Fe–15Cr alloys (as dictated by the acting thermodynamic driving forces). This result is by no means obvious, since the cascade time-scale is very short compared to typical thermodynamic time-scales. There are previous reports of thermodynamic effects affecting cascade outcome; however, the heats of mixing in those cases were much larger than in the present one [41]. The absolute change of the SRO parameter (as well as the absolute value of the mixing enthalpy) is larger in an Fe–15Cr alloy. In Fe–5Cr alloys the process responsible for the induced SRO is the break up of Cr–Cr nn pairs, whereas in the case of an Fe–15Cr alloy analysis of the SRO parameter is not enough to conclude whether there is growth of pre-existing Cr clusters, new clusters are formed, or whether both processes occur at the same time.

Concerning the effect of possible defect segregation in Fe–Cr alloys with Cr-rich precipitates, as stated in Section 3.2.1, the formation energy of both vacancy and self-interstitial defects is higher in the precipitate than in the matrix. Because of this, fast mobile self-interstitial defects were observed to escape from the precipitate. We expect that vacancy defects initially created inside the precipitate should also move to the matrix, however, this cannot be observed within the time frame of an MD run. Thus, accumulation of both types of defects is expected to occur near the precipitate matrix interface, wherein they should recombine. It is therefore tempting to speculate that on the long term time-scale precipitates may act as sinks for mobile defects and their presence should lead to the reduction of the damage produced.

## 5. Conclusions

We have studied displacement cascades using MD simulations in random Fe–Cr alloys with  $C_{Cr} = 5, 10, \text{ and } 15\%$ , with and without Cr-rich precipitates, to investigate possible effects of the Cr concentration on the primary damage state. The following conclusions can be drawn based on the results obtained:

- (i) The variation of the Cr concentration has no effect on the amount of survived Frenkel pairs, nor on the distribution of defects in clusters, as compared to results obtained in pure Fe. The only noticeable effect of the Cr content on the cascade-induced defects is seen in the enrichment of Cr in survived SIAs, depending on the Cr content, the PKA energy and also the potential applied.
- (ii) The analysis of the SRO parameter in matrices subjected to 5 keV cascades reveals Cr ordering in Fe–5Cr (negative SRO) and Cr clustering in Fe–15Cr (positive SRO) alloys, as dictated by the acting thermodynamic driving forces.
- (iii) The comparative study of cascades in Fe–10Cr matrices, with and without Cr-rich precipitates, shows that the number of surviving defects and clustered fractions are not changed by the presence of the precipitates. In turn, pre-existing 5 nm precipitates are not dissolved or modified in any significant way by 20 keV cascades. However, SIAs and SIA clusters initially formed inside the precipitates are observed to migrate from the precipitates towards the precipitate–matrix interface, while cascades are observed to split more easily as a consequence of the presence of the precipitates. It can therefore be concluded that the main effect of the precipitate on the primary damage is the increase of self-interstitial defects attached to the precipitate–matrix interface, as the higher number of subcascades induces only a negligibly higher number of produced defects.

## Acknowledgements

This work, supported by the European Communities under the contracts of Association between EURATOM/Tekes and EURATOM/SCK-CEN, was carried out within the framework of the European Fusion Development Agreement. Partial support was also received from the EURATOM 7th framework programme, under grant agreement number 212175 (GetMat project). The research was performed within the Finnish Centre of Excellence in Compu-

tational Molecular Science (CMS), financed by the Academy of Finland and the University of Helsinki.

## References

- [1] L.K. Mansur, A.F. Rowcliffe, R.K. Nanstad, S.J. Zinkle, W.R. Corwin, R.E. Stoller, *J. Nucl. Mater.* 329–333 (2004) 166.
- [2] M.L. Jenkins, C.A. English, B. Eyre, *Philos. Mag. A* 38 (1979) 97.
- [3] E.A. Little, D.A. Stow, *J. Nucl. Mater.* 87 (1979) 25.
- [4] E.A. Little, R. Bullough, M. Wood, *Proc. R. Soc. London A* 372 (1980) 565.
- [5] F.A. Garner, M.B. Toloczko, B.H. Sencer, *J. Nucl. Mater.* 276 (2000) 123.
- [6] S.J. Zinkle, *Phys. Plasmas* 12 (2005) 058101.
- [7] B.D. Wirth, M.J. Caturla, T. Diaz de la Rubia, T. Khraishi, H. Zbib, *Nucl. Instrum. and Meth. B* 180 (2001) 23.
- [8] L. Malerba, *J. Nucl. Mater.* 351 (2006) 28.
- [9] A.F. Calder, D.J. Bacon, *Mater. Res. Soc. Symp.* 439 (1997) 521.
- [10] A.F. Calder, D.J. Bacon, A.V. Barashev, Y.N. Osetsky, *Philos. Mag. Lett.* 88 (2008) 43.
- [11] C.S. Becquart, C. Domain, J.C. Van Duysen, J.M. Raulot, *J. Nucl. Mater.* 294 (2001) 274.
- [12] D. Terentyev, L. Malerba, R. Chakarova, C. Domain, K. Nordlund, P. Olsson, M. Rieth, J. Wallenius, *J. Nucl. Mater.* 349 (2006) 119.
- [13] C. Björkas, K. Nordlund, L. Malerba, D. Terentyev, P. Olsson, *J. Nucl. Mater.* 372 (2008) 312.
- [14] L. Malerba, D. Terentyev, P. Olsson, R. Chakarova, J. Wallenius, *J. Nucl. Mater.* 329–333 (2004) 1156.
- [15] J.-H. Shim, H.-J. Lee, B.D. Wirth, *J. Nucl. Mater.* 351 (2006) 56.
- [16] J. Wallenius, P. Olsson, C. Lagerstedt, N. Sandberg, R. Chakarova, V. Pontikis, *Phys. Rev. B* 69 (2003) 094103.
- [17] F. Willaime, C.C. Fu, M.C. Marinica, J. Dalla Torre, *Nucl. Instr. Meth. Phys. Res. B* 228 (2005) 92.
- [18] P. Olsson, I. Abrikosov, L. Vitos, J. Wallenius, *J. Nucl. Mater.* 321 (2003) 84.
- [19] P. Olsson, A.I. Abrikosov, J. Wallenius, *Phys. Rev. B* 73 (2006) 104416.
- [20] P. Olsson, J. Wallenius, C. Domain, K. Nordlund, L. Malerba, *Phys. Rev. B* 72 (2005) 214119.
- [21] D. Terentyev, P. Olsson, T.P.C. Klaver, L. Malerba, *Comput. Mater. Sci.* (2008), doi:10.1016/j.commatsci.2008.03.013.
- [22] I. Mirebeau, M. Hennion, G. Parette, *Phys. Rev. Lett.* 53 (1984) 687.
- [23] P. Dubuisson, D. Gilbon, J.L. Séran, *J. Nucl. Mater.* 205 (1993) 178.
- [24] M.H. Mathon, Y. de Carlan, G. Geoffroy, X. Averty, A. Alamo, C.H. de Novion, *J. Nucl. Mater.* 312 (2003) 236.
- [25] N.P. Filippova, V.A. Shabashov, A.L. Nikolaev, *Phys. Met. Metall.* 90 (2000) 145.
- [26] O.K. Andersen, T. Saha-Dasgupta, *Phys. Rev. B* 62 (2000) R16219.
- [27] G. Kresse, D. Joubert, *Phys. Rev. B* 59 (1999) 1758.
- [28] P. Blöchl, *Phys. Rev. B* 50 (1994) 17953.
- [29] K. Nordlund, 2006, *PARCAS* computer code. The main principles of the molecular dynamics algorithms are presented in [42,43]. The adaptive time step and electronic stopping algorithms are the same as in [44].
- [30] M.P. Allen, D.J. Tildesley, *Computer Simulation of Liquids*, Oxford University Press, Oxford, England, 1989.
- [31] In a related study, we have compared cascades of the same initial recoil energy run with and without electronic stopping [45]. We found that the total amount of damage scales linearly with the nuclear deposited energy (the initial recoil energy minus the energy deposited to electronic stopping).
- [32] H.J.C. Berendsen, J.P.M. Postma, W.F. van Gunsteren, A. DiNola, J.R. Haak, *J. Chem. Phys.* 81 (1984) 3684.
- [33] J.M. Cowley, *Phys. Rev.* 77 (1950) 669.
- [34] C.S. Becquart, C. Domain, A. Legris, J.-C.V. Duysen, *J. Nucl. Mater.* 280 (2000) 73.
- [35] G.J. Ackland, M.I. Mendelev, D.J. Srolovitz, S. Han, A.V. Barashev, *J. Phys. Condens. Matter* 16 (2004) S2629.
- [36] D. Terentyev, L. Malerba, M. Hou, *Phys. Rev. B* 75 (2007) 104108.
- [37] D. Terentyev, L. Malerba, A.V. Barashev, *Philos. Mag. Lett.* 85 (2005) 587.
- [38] D. Terentyev, P. Olsson, L. Malerba, A.V. Barashev, *J. Nucl. Mater.* 362 (2007) 167.
- [39] R.S. Averback, T. Diaz de la Rubia, *Displacement damage in irradiated metals and semiconductors*, in: H. Ehrenfest, F. Spaepen (Eds.), *Solid State Physics*, vol. 51, Academic, New York, 1998, p. 281.
- [40] D.J. Bacon, A.F. Calder, F. Gao, V.G. Kapinos, S.J. Wooding, *Nucl. Instrum. and Meth. B* 102 (1995) 37.
- [41] T.J. Colla, H.M. Urbassek, K. Nordlund, R.S. Averback, *Phys. Rev. B* 63 (2000) 104206.
- [42] K. Nordlund, M. Ghaly, R.S. Averback, M. Caturla, T. Diaz de la Rubia, *J. Tarus, Phys. Rev. B* 57 (1998) 7556.
- [43] M. Ghaly, K. Nordlund, R.S. Averback, *Philos. Mag. A* 79 (1999) 795.
- [44] K. Nordlund, *Comput. Mater. Sci.* 3 (1995) 448.
- [45] C. Björkas, K. Nordlund, manuscript in preparation.